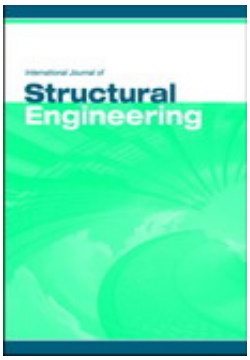

International Journal of Structural Engineering

ISSN online: 1758-7336 - ISSN print: 1758-7328
https://www.inderscience.com/ijstructe

Tensile characterisation of semi-cured epoxy-impregnated FRCM using digital image correlation technique

Nikhil Holsamudrkar, Sauvik Banerjee, Asim Tewari

DOI: 10.1504/IJSTRUCTE.2024.10062425

Article History:

Received:	28 August 2023
Last revised:	06 November 2023
Accepted:	13 November 2023
Published online:	26 February 2024

Tensile characterisation of semi-cured epoxy-impregnated FRCM using digital image correlation technique

Nikhil Holsamudrkar and Sauvik Banerjee*

Department of Civil Engineering,
Indian Institute of Technology, Bombay,
Mumbai, 400076, India
Email: nikhil.nnh@gmail.com
Email: sauvik@civil.iitb.ac.in
*Corresponding author

Asim Tewari

Department of Mechanical Engineering,
Indian Institute of Technology,
Bombay, Mumbai,
400076, India
Email: asim.tewari@iitb.ac.in

Abstract: The progress made in developing FRCM over the past two decades has demonstrated that epoxy coating before embedding fibres in a mortar matrix enhances the mechanical properties of the composites by preventing fibre-fibre slippage. However, this epoxy makes the fabric stiff; unsuitable for curved surfaces. The previous attempts made by researchers to introduce prepreg fabric into concrete/mortar reduce the fabric exploitation ratio and also raise durability concerns. In this study, an on-site impregnation approach is proposed, which involves semi-curing the fabric with epoxy to achieve a certain degree of cure before incorporating it into a cementitious matrix without affecting bendability. The parameters considered in the study include the type of fibre mesh and the degree of epoxy cure at the time of placement. A direct tensile characterisation of both pristine and impregnated fibres, as well as FRCM composites, is conducted. The results indicate that semi-cured methodology shows improvement in tensile strength over uncured ones, by 16.5% and 6.4% for leno and plain weave, respectively.

Keywords: fibre-reinforced cementitious matrix; FRCM; TRM; tensile characterisation; semi-cure; on-site repair; differential scanning calorimetry; DSC; laser Raman spectroscopy; LRS; degree of cure; DOC.

Reference to this paper should be made as follows: Holsamudrkar, N., Banerjee, S. and Tewari, A. (2024) 'Tensile characterisation of semi-cured epoxy-impregnated FRCM using digital image correlation technique', *Int. J. Structural Engineering*, Vol. 14, No. 1, pp.84–111.

Biographical notes: Nikhil Holsamudrkar is presently pursuing his Doctorate under the supervision of Professor Sauvik Banerjee in the Department of Civil Engineering at the Indian Institute of Technology Bombay (IITB). His research focuses on various aspects of structural engineering, encompassing topics such as strengthening with fibre reinforced polymers (FRP), the use of FRP as internal reinforcement, fibre reinforced cementitious matrix (FRCM) strengthening, AIML-based data analysis, and structural health monitoring through methods like acoustic emission (AE) and digital image correlation (DIC).

Sauvik Banerjee is currently a Professor of Structural engineering in the Department of Civil Engineering, Indian Institute of Technology Bombay (IITB). Prior to joining IITB, he spent three years as an assistant professor at the Parks College of Engineering, Aviation and Technology, Saint Louis University, USA. His research interests includes structural health monitoring (SHM) using wave propagation and vibration based approaches, ultrasonic nondestructive evaluation (NDE) and imaging of materials, elastodynamic modelling of advanced composite structures, condition assessment of structures using NDT, passive acoustic emission (AE) monitoring of structures, FRP retrofitting of structures, and impact response of structures.

Asim Tewari is a Professor in the Department of Mechanical Engineering and a faculty member of the Center for Machine Intelligence and Data Science (C-MInDS) at the Indian Institute of Technology Bombay, Mumbai. He graduated with a BTech from the IIT Kanpur, followed by an MS and PhD from the Georgia Institute of Technology, Atlanta. His area of research is in mathematical models for microstructural mechanics and applied machine learning. He has over 100 international journal and conference publications and ten international and four Indian patent research funding of over 15 million USD.

1 Introduction

The strengthening of concrete and masonry structures involves the utilisation of different methodologies and materials, such as steel plates and sections, RCC jacketing, engineered cementitious composites (ECC) overlays, and fibre-reinforced polymers (FRP). Externally bonded FRP has become immensely popular due to its easy on-site application to various structural members and the availability of design codes (American Concrete Institute, 2017). However, FRP has limitations, including substrate debonding, inapplicability to wet substrates, and higher costs. To overcome some of these limitations, fibre-reinforced cementitious matrix (FRCM) composites have been introduced. FRCM offers advantages such as improved bond compatibility even in wet conditions, resistance to high temperatures, lower costs, moisture breathability post-strengthening, and a smooth surface finish. FRCM comprises technical textiles acting as reinforcement, such as polyphenylene, benzobisoxazole (PBO), carbon, basalt, and glass, embedded in cement or lime-based mortars as matrices.

Numerous studies have demonstrated the efficacy of FRCM in the flexural strengthening of beams (Escrig et al., 2017; Ombres, 2011; D'Ambrisi and Focacci,

2011), dapped-end beams retrofitting (Ferreira et al., 2023), shear strengthening (Al-Salloum et al., 2012; Tetta et al., 2016), and column confinement (Guo et al., 2022; Ombres, 2014; Tsesarsky et al., 2013; Tello et al., 2023). The latest trend in the FRCM domain revolves around the coating of fibres to enhance the fibre-fibre and fibre-matrix bond. Research indicates that coating the fibres with inorganic silica, such as micro-silica (Nadiv et al., 2017) or nano-silica (Dvorkin and Peled, 2016; Signorini et al., 2018), improves the tensile strength of FRCM by enhancing the fibre-fibre bond. Also, it has been found that applying an SBR latex coating on carbon fabric degrades the flexural strength and toughness of FRCM (Halvaei et al., 2018). Conversely, an epoxy coating comprising 35–100% by weight of the fabric has been shown to increase post-cracking strength by 70-190% and flexural toughness by 250–780% (Donnini et al., 2016). Another study investigated the effect of different impregnation levels of epoxy on direct tension, pull-off, and shear bond tests, as well as the impact of interface roughness on the overall response (Donnini et al., 2016). The results demonstrated that epoxy coating significantly improves tensile strength and shear bond strength with masonry, while interface roughness has a notable influence on the composite's failure mode and performance. Several other researchers have also showcased improvements in the mechanical properties of epoxy-coated FRCM composites (Signorini et al., 2020; Zhu et al., 2023).

Furthermore, the effect of fabric geometry has been investigated, indicating that woven fabrics are more efficient than knitted weft insertion fabrics (Peled and Bentur, 2000). Surprisingly, an epoxy coating on knitted fabrics, specifically leno weave, increased the tensile strength of the fabric by 90-100% due to effective stress redistribution among the knit fibre filaments (D'Antino et al., 2020). To achieve the characteristic tri-linear composite response and promote multi-cracking behaviour when utilising textiles as reinforcement, it is advisable to employ a stiffer epoxy coating with low viscosity (Rampini et al., 2021).

In an attempt to achieve bendability, thermoplastic polymer coating was used by (Heins et al., 2023) and found to have competitive performance compared to SBR latex coating. Also, the first attempt to introduce prepreg in FRCM was done by (Scheurer et al., 2022). The authors found that the concrete environment affects the curing process of the pre-impregnated textiles and thereby reduces their tensile strength compared to fully cured epoxy-impregnated specimens. The authors also found optimum performance with water-dispersed epoxy resin.

2 Research significance

In spite of numerous prior investigations into the epoxy impregnation for FRCM, the inherent stiffness presents substantial challenges when attempting to apply the FRCM on curved surfaces or areas with bends. An alternative approach, pre-impregnation, has been considered to address this issue. However, this method significantly reduces the fabric exploitation ratio, as documented in the literature (Scheurer et al., 2022), and raises other concerns such as durability, and dependency on specific formulations of the epoxy thereby increasing cost. To tackle these challenges, this research introduces an on-site semi-cure technique for epoxy-impregnated fabric. The study emphasises the use of readily available diglycidyl ethers of bisphenol A (DGEB) resin in combination with an amine-based hardener, chosen for its cost-efficiency. Integral to this investigation

are considerations of fabric type and the initial degree of epoxy curing, recognised as pivotal parameters. The study effectively determines the optimal initial degree of cure (DOC) necessary prior to fabric placement, aimed at achieving the highest possible fabric exploitation ratio without compromising the bendability of the fabric.

Two fabric geometries, namely a unidirectional (UD) plain (woven) and a bidirectional (BD) leno (knitted), are employed in the study. The initial degree of epoxy cure is categorised as uncured, semi-cured, and fully cured. Differential scanning calorimetry (DSC) is used to optimise the DOC, while laser Raman spectroscopy (LRS) investigates how the presence of water in the mortar affects the curing kinetics of epoxy with different initial DOC values.

Moreover, a comprehensive evaluation of the mechanical performance of the fabric and FRCM composite is conducted through direct tension tests for the said parameters. To further investigate the behaviour of leno semi-cured FRCM specimens, they are subjected to temperatures of 100°C, 150°C, and 200°C for a duration of 24 hours. The stress-strain response during the tests is monitored using the digital image correlation (DIC) technique. Additionally, the stress-strain behaviour of the FRCM composite is modelled using established models in the available literature, such as the modified Aveston Cooper Kelly (ACK) model and the modified tension-stiffening model. The models are adapted to incorporate a damage coefficient for different initial degrees of cure (DOC).

3 Experimental program

3.1 Materials

3.1.1 Textile

A leno carbon fabric weighing 400 GSM and a mesh size of 15 mm was employed. In this mesh, two 12K yarns were knitted with a wavy pattern in the warp direction, while a single 24K yarn was inserted between the warp bundle to provide fabric stability. The authors developed a UD carbon plain weave fabric 160 GSM, 6 mm warp spacing for cost-effectiveness. The plain fabric consists of 24K straight carbon yarns in the warp direction and nylon in the weft direction. The nylon was pre-heated at 100°C for bonding with the carbon yarns and to enhance fabric stability. The properties of the source yarn are presented in Table 1, and images of the fabric are shown in Figure 1.

Table 1 Properties of the source yarn

	Fabric type	*Tensile strength (MPa)*	*Modulus (GPa)*	*Elongation (%)*	*Density (g/m^3)*	*Filament diameter (μm)*
Manufacturer	Plain	2516	250	2.2	1.8	7
Lab derived		1660.1	95.5	2.3	-	-
Lab derived	Leno	1682.4	80.9	2.4	-	-

Figure 1 (a) Leno knitted fabric (b) Plain weave fabric

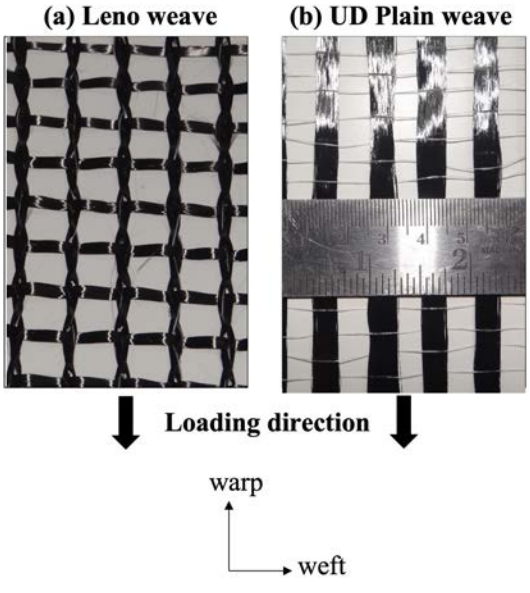

3.1.2 Cementitious mortar

Standard non-shrink repair mortar was used as a cementitious matrix. A water-to-mix ratio of 0.16 was adopted throughout the study. Flexural tests were conducted at the Structural Evaluation and Material Testing Lab, as per European Committee for Standardization (2016), and an average of five specimens were reported. As per the code, 40 × 40 × 160 mm beams were cast and tested at a 50 N/s rate in load control. Once the beam broke into two pieces, these were again tested using a compression jig at 2,400 N/s rate to determine compressive strength. The overall properties are shown in Table 2.

Table 2 Mechanical properties of the cementitious matrix

	Compressive strength 28 days (MPa)	*Flexural strength (MPa)*	*Modulus (GPa)*	*Bond strength to concrete (MPa)*
Manufacturer	65.0	9.0	>30.0	>2.0
Lab derived	68.5	5.9	28.6	-

3.1.3 Epoxy

DGEB resin and an amine-based hardener were employed in the investigation. The properties provided by the manufacturer are given in Table 3.

Table 3 Properties of the epoxy as provided by manufacturer

Mixing ratio by weight	*Initial mix viscosity at 25°C (ASTM D2196)*	*Pot life at 25°C (ASTM D2471)*	*Curing schedule*	*Tensile strength (ISO 527)*	*Modulus (ISO 527)*	*Elongation (ISO 527)*
DGEB: 10 TETA: 1	30–40 min.	5,000–8,000 m Pas	25°C – 24 hrs. 80°C – 60 min. 140°C – 10 min.	55–70 MPa	2.5–4 GPa	1.5–3%

Figure 2 (a) (b) LY specimens prepared with UC, SC strategies cured underwater (c) Specimens prepared for LRS (d) DSC setup (e) LRS setup (see online version for colours)

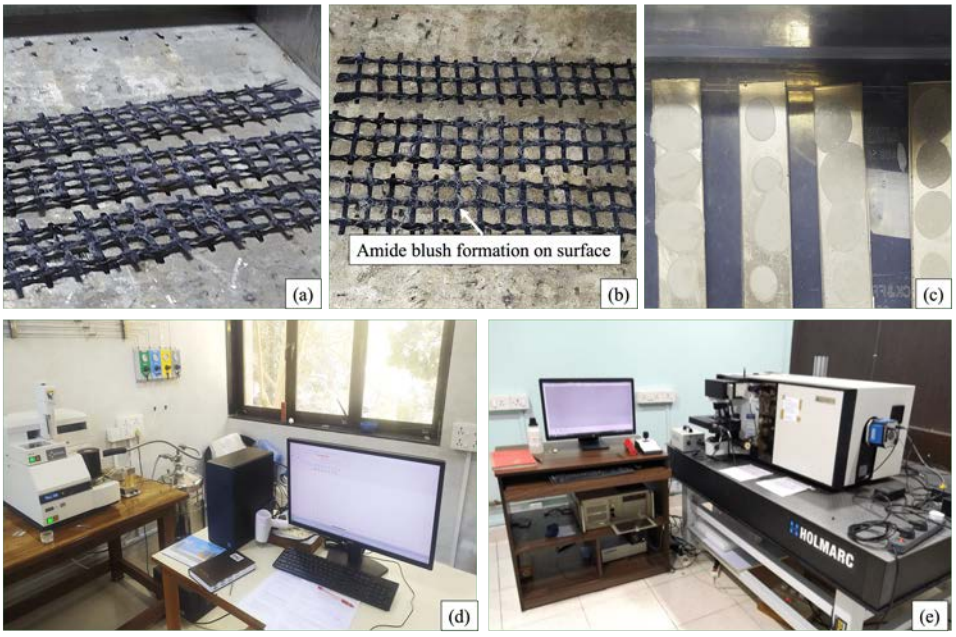

3.2 Specimen preparation and mechanical testing

3.2.1 Single yarn and fabric

Single yarn and fabric coupons were prepared using aluminum tabbing, following the guidelines specified in ASTM standards (ASTM International, 2017, 2008). The study employed two strategies: uncured (UC) and semi-cured (SC). The UC strategy involved placing uncured epoxy-impregnated fabric in the water. Similarly, SC specimens achieve a certain DOC for epoxy-impregnated fabric before placing it in water. Throughout the investigation, it was assumed that only water in the mortar significantly affected the curing kinetics and mechanical properties of the epoxy. For the preparation of specimens using the UC and SC strategies, the samples were coated and then immersed in water for 14 days in a controlled environment [see Figures 2(a)–2(b)]. Fully cured (FC) samples, on the other hand, were coated and subjected to air curing for

24 hours. The cementitious matrix was sieved using a 300 μm sieve and used to prepare mortar-impregnated coupons. These samples were cured for 24 hours in a humidity-controlled chamber with a relative humidity of 99.9%, followed by seven days of underwater curing. Testing was conducted one day after ensuring that all specimens were thoroughly air-dried.

Table 4 Single yarn and fabric test protocols as per ASTM International (2017, 2008)

	Gauge length (mm)	*Fabric width (mm)*	*Rate of loading (mm/min)*	*Preload ($\mu\varepsilon$)*	*Grip pressure (MPa)*	*Grip length (mm)*
Plain source yarn	75	-	0.5	100	10	75
Leno yarn	75	-	0.5	100	15	75
Leno/plain fabric	75	50	0.5	100	15	75

A two-letter notation system was utilised, where the first letter denoted the type of fabric (L/P for leno/plain), and the second letter indicated whether it was a yarn or fabric specimen (Y/F). Also, leno yarn was referred to as the 'LY pair' since it was tested as a twisted yarn pair. It was observed that the extensometer was ineffective in capturing the strain data. Hence, only actuator displacement was used for pristine and mortar-impregnated fabric samples. Please refer to Table 4 for the test protocols used in testing yarn and fabric.

3.2.2 FRCM composite

Tensile coupons were produced using a layered mold, as illustrated in Figure 3. UC and SC specimens were coated according to their respective strategies and immediately inserted between the mortar layers. After casting, the mold was covered with plastic to prevent moisture loss and transferred to a controlled curing chamber for a duration of 28 days. The dried specimens were tabbed with carbon FRP and cured at room temperature for 24 hours. The L-SC-HT category samples underwent heating at temperatures of 100°C, 150°C, and 200°C in an oven for 24 hours after the completion of the curing period and full drying of the samples (Trapko, 2013). It is worth noting that the heating scheme is not standard and varies across the literature (Trapko, 2013; Messori et al., 2019; Ombres, 2014). In this study, the choice of temperature is determined with a focus on applications in environments with elevated ambient temperatures, such as industrial facilities equipped with ovens. The samples were removed from the oven after gradually cooling to room temperature. Testing was conducted at the Advanced Mechanical Testing Facility (AMTF), one or two days after the tabbing process.

For tensile characterisation, an articulated clevis grip tensile testing setup similar to the one used at Cracow University of Technology (CUT), Cracow, Poland was adopted (Hojdys and Krajewski, 2021; ICC Evaluation Services Inc., 2016; Younis et al., 2020). Quasi-static tensile tests were performed at a constant displacement rate of 0.5 mm/min referring to (ICC Evaluation Services Inc., 2016). The non-contact-based strain was monitored using a commercially available digital image correlation (DIC) package by Correlated Solutions. The Basler acA2440-75uc USB 3.0 camera incorporating the Sony IMX250 CMOS sensor was used. It offers a 2/3" sensor format and a physical size of 8.4 mm $\times$ 7.1 mm with a resolution of 5 MP (2,448 px $\times$ 2,048 px). A Nikon 50 mm

lens with f/1.2 was used with the camera to provide sharp images. The photos were captured using VIC-Snap at a sampling rate of 2 Hz, and the results were analysed and post-processed using VIC-2D with a subset size of 45 pixels. To synchronise the DIC data with the load data from the actuator (MTS Systems Corporation, Landmark 100 kN Servo Hydraulic system), a data acquisition system from National Instruments Corp. (NI USB-6221, 16-bit, 0.25 MSPS) was used. This system converted voltage input from the actuator to load data. The surface of the specimens was smoothened with 120 grit sandpaper to remove any unevenness, followed by priming with white matte finish paint and subsequently applying black speckle paint. A constant gust of spray was applied to the surface until a uniform speckle pattern was achieved. A Hedler 1000 non-flickering LED light source was utilised, and its intensity was adjusted based on the focusing inputs provided by VIC-SNAP. The testing was conducted in a controlled environment to prevent image distortion caused by the heating of the light source. Detailed information about the setup is provided in Figure 4.

Figure 3 FRCM tensile specimen casting specifications (see online version for colours)

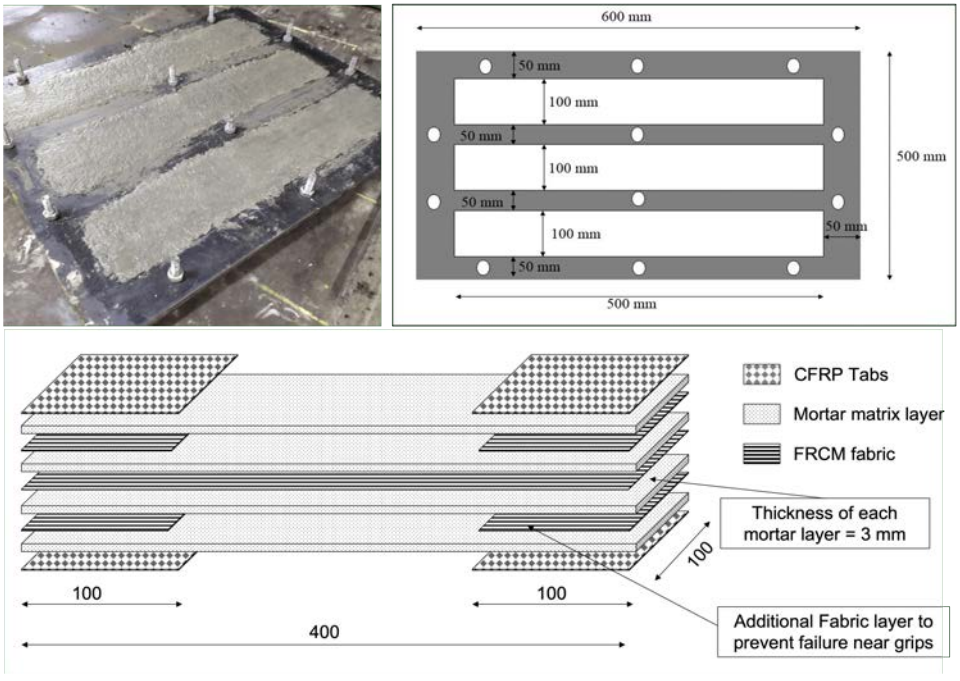

The nomenclature used for all specimens followed the pattern X-Y-N, where X represents the initial letter of the fabric type, Y denotes the condition of the fabric (Pristine/UC/SC/FC), and N indicates the specimen number. An additional category, called intersection coated (IC), was also included for leno fabric, which will be further explained in the study. High-temperature exposed leno semi-cured specimens are denoted as L-SC-HT100-N, where 100 indicates the temperature in degrees Celsius.

Figure 4 Tensile characterisation test setup, (a) MTS landmark hydraulic system (b) lighting source (c) CCD camera (d) MTS acquisition system (e) DIC system (f) speckle pattern (g) articulated clevis grip setup as per CUT* (h) detailed setup (see online version for colours)

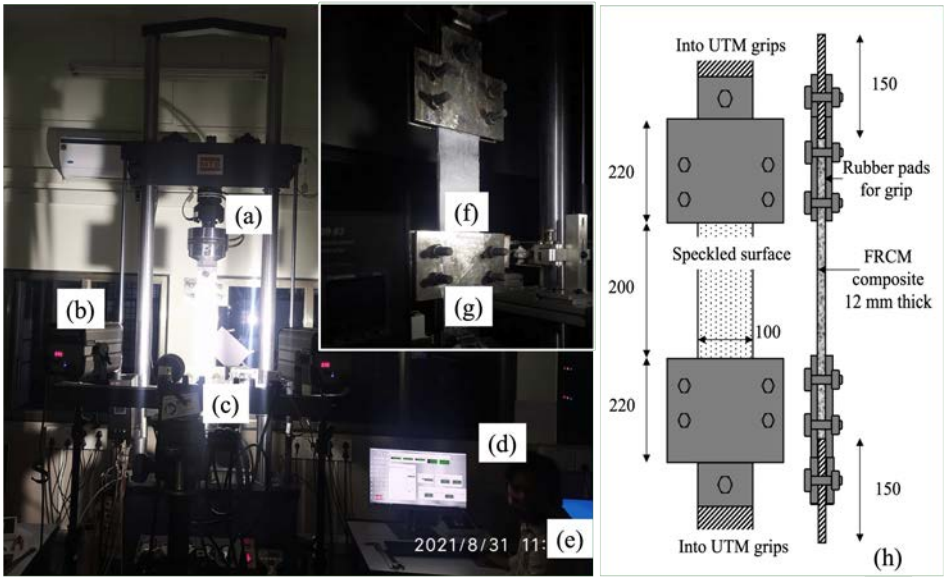

Source: *Hojdys and Krajewski (2021)

3.2.3 Digital image correlation

The current study utilises zero mean normalised sum of square difference (ZNSSD) criteria for DIC analysis, which is unaffected in the case of offset or uneven lighting conditions. Let $f_1(x_i, y_i)$ and $f_2(x_i', y_i')$ indicate the grey values of the i th pixel of the reference and target subsets, respectively, for a square subset comprising $n(N \times N)$ discrete pixels. The grey values of $f_1(x_i, y_i)$ and $f_2(x_i', y_i')$ are further representated as f_{1i} and f_{2i}. Coefficient C_{ZNSSD} is minimised for every search conducted, given by:

$$C_{ZNSSD} = \sum \left(\frac{\bar{f}_{1i}}{\sqrt{\sum \bar{f}_{1i}^2}} - \frac{\bar{f}_{2i}}{\sqrt{\sum \bar{f}_{2i}^2}} \right)^2. \quad (1)$$

3.3 Microstructural characterisation

3.3.1 DSC and LRS

DSC was performed on four samples, where one sample underwent a dynamic scan ranging from 20°C to 300°C, and the remaining three samples underwent isothermal scans at temperatures of 80°C, 100°C, and 150°C. The epoxy was prepared at the facility and immediately transferred to the Hitachi DSC7020 machine for analysis. Mixing of epoxy was done for 4 minutes. The DSC testing was conducted at the TGDTA

Lab, with a scanning rate of 10°C/min. A nitrogen atmosphere with a flow rate of 50 ml/min and a sampling rate of 5 Hz was maintained during the DSC measurements.

For LRS, epoxy specimens were prepared using the UC, SC, and FC strategies followed by underwater curing at room temperature for 14 days, as shown in Figure 2(c). After complete drying, the specimens were transferred to the LRS facility. The Horiba Jobin Yvon HR800-UV confocal micro-Raman spectrometer was utilised for LRS measurements, employing an excitation source with a wavelength of 532 nm and a power of 50 mW. Two spots were scanned for each specimen.

3.3.2 ESEM

Environmental scanning electron microscopy (ESEM) samples were obtained from the fabric of FRCM composite specimens that experienced failure. Scanning was done using an electron microscope (FEI Quanta 200), which is housed in the ESEM facility at the central facilities. The imaging was carried out under high vacuum conditions (Vacuum pressure 60 Mpa, voltage 15 kV, filament current 2.59 A, emission current 105 μA). Each sample underwent sputter coating before placing in the ESEM.

4 Results and discussion

4.1 Mechanical characterisation

4.1.1 Single yarn and fabric

PY and PF exhibit typical linear stress-strain responses, while the LY pair shows load-displacement behaviour, as shown in Figure 5(a), with two distinct peaks for both twisted yarns, resulting in a reduction of ultimate strength (σ_u) to 883.8 MPa with a COV of 14.8%. The elongation of the yarns occurs progressively due to uneven looseness, resulting in two peak formations. The first peak corresponds to the load-bearing capacity of relatively straight filaments, while the second peak corresponds to the stretching and failure of the remaining loose filaments. This phenomenon is referred to as 'looseness' and is quantified as the difference in peak displacement of yarn pairs (L_r) as shown in Figure 5(a). Notably, the looseness (L_r) varies depending on the location of the yarn pair across the width and length of the fabric, indicating a non-uniform parameter within the material. This variation was confirmed by testing multiple LY pairs across the fabric width [Figure 5(a)]. A similar behaviour was reported by D'Antino et al. (2020), where the capacity of leno fabric was found to be approximately 50% in pristine condition compared to impregnated ones.

LY pair with intersection coating (IC) are the specimens with epoxy coating only at the warp-weft junction thereby preserving fabric bendability. Despite the stiffness imparted by epoxy, it exhibited a response similar to that of the LY pair, with a σ_u of 765.2 MPa and a COV of 10.1%. On the other hand, LY pairs impregnated with a mortar matrix experienced a reduction in σ_u to 462.1 MPa with a COV of 8.1%, indicating the rubbing of loose fibre filaments against the cured mortar and subsequent local shear failure of some filaments as the main contributing factors to this reduction [Figure 5(c)].

The behaviour of LF in pristine conditions becomes complex due to the involvement of multiple yarn pairs in the failure mechanism, as depicted in Figure 5(b). Initially, a

few yarns undergo stretching, leading to initial seating behaviour, followed by a linear stress-strain response. The post-peak behaviour can be attributed to the progressive stretching and failure of the remaining loose yarns. The σ_u for LF was found to be 1079.1 with a COV of 11.4%. In comparison, PF exhibited an average strength of 1705.8 with a COV of 1.7% in pristine conditions. Overall, the summary for plain and leno fabrics in pristine condition [Figure 5(b)] reveals that LY and LF exhibit approximately half the capacity of PY and PF, despite having similar source yarn properties (Table 1). The leno fabric specimens demonstrated higher elongation at failure (ϵ_f) of 4.7-5.9% compared to PY specimens (1.8-2.4%) due to looseness in the fabric.

Table 5 Test matrix for yarn and fabric specimens

Specimen ID	*No. of specimens*	σ_u *(MPa)*		E_f *(GPa)*		ϵ_f *(%)*	
		Avg.	*COV (%)*	*Avg.*	*COV (%)*	*Avg.*	*COV (%)*
PY pristine	3	1,660.1	4.6	95.5	4.9	2.4	3.2
PY epoxy impregnated UC	3	1,789.1	3.7	105.2	3.0	1.8	3.8
PY epoxy impregnated SC	3	1,855.4	2.6	104.5	4.4	2.0	3.4
PY epoxy impregnated FC	3	1,970.0	1.7	106.1	1.8	1.9	6.7
PF pristine	2	1,705.8	1.7	96.8	1.5	2.1	0.2
LY pair pristine	8	883.8	14.8	-	-	5.9	19.9
LY pair intersection coated (IC)	3	765.2	10.1	-	-	5.6	15.2
LY pair mortar impregnated	3	462.1	8.1	-	-	4.7	0.5
LY pair epoxy impregnated UC	3	1,605.1	4.8	95.3	4.9	2.1	2.6
LY pair epoxy impregnated SC	3	1,783.4	2.5	93.4	5.8	2.2	3.2
LY pair epoxy impregnated FC	3	1,882.6	1.5	95.9	6.2	2.4	1.6
LF pristine	5	1,079.1	11.4	76.2	14.4	5.0	28.4

LY specimens prepared with uncured (UC), semi-cured (SC), and fully cured (FC) strategies exhibited a significant improvement in mechanical strength, approximately 110% higher than the pristine ones [Figure 5(c)]. The target degree of curing (DOC) value for the SC strategy was determined from the differential scanning calorimetry (DSC) results, explained in the 4.3.1. The increase in curing degree from UC to FC increased σ_u from 1,789.1 to 1,970.0 MPa for PY and 1,605.1 to 1,882.6 MPa for LY. Interestingly, the modulus (E_f) values remained the same for both PY and LY, indicating no influence of initial curing degree on modulus. Epoxy impregnation eliminated the two-peak behaviour and resulted in a final capacity approximately twice that of the LY pair in pristine conditions. Detailed results are presented in Table 5.

4.1.2 FRCM composite

The results of all FRCM specimens are presented in Figures 6, 8 and 9, which display the stress-strain response for each specimen. Additionally, detailed behaviour for one of the specimens is explained, highlighting the crack width evolution and variation of e_{yy} and V along the specimen's length. For each specimen type, three points are selected: P_1 indicates the appearance of the first crack or matrix cracking, P_2 represents the crack growth stage, and P_3 corresponds to the failure stage. To monitor individual cracks at these points, Figures 7 and 10 are referred to. These figures contain corresponding DIC images.

Table 6 Test matrix for FRCM composites

Specimen ID	*No. of specimens*	σ_1 *(MPa)*		σ_3 *(MPa)*		E_3 *(GPa)*		ϵ_u *(%)*		C_s *(mm)*		C_w *(mm)*		*Failure mode*
		Avg.	*COV (%)*	*Avg.*	*COV (%)*	*Avg.*	*COV (%)*	*Avg.*	*COV (%)*	*Avg.*	*COV (%)*	*Avg.*	*COV (%)*	
L-P	4	406.2	1.8	554.9	9.9	0.1	26.6	2.6	4.3	51.6	9.8	5.8	4.0	FP
L-IC	3	430.2	1.6	613.8	12.3	-	-	2.9	8.6	66.1	5.3	4.5	2.8	FP
L-UC	3	392.8	2.3	1,267.1	2.7	84.6	13.8	1.7	3.2	20.1	18.3	0.7	4.2	FR
L-SC	3	394.9	2.1	1,476.8	5.2	81.2	10.2	2.0	2.4	15.2	10.8	0.5	5.6	FR
L-FC	3	481.9	1.8	1,588.4	9.1	83.8	8.4	1.7	8.1	26.1	6.7	0.9	4.7	FR
L-SC-HT100	3	279.2	4.5	1,467.2	8.5	83.4	4.3	1.8	4.8	19.3	10.1	0.8	3.1	FR
L-SC-HT150	3	290.1	5.2	1,466.5	2.9	84.1	3.6	1.9	3.3	18.7	12.6	0.7	2.3	FR
L-SC-HT200	3	207.3	4.9	1,237.6	8.6	49.8	3.2	2.1	3.8	41.8	8.2	10.8	21.3	FMD
P-P	3	590.8	3.1	1,381.5	4.9	84.7	6.5	1.3	8.1	23.6	13.9	0.7	3.2	FFS
P-UC	3	560.2	4.3	1,605.5	1.3	88.1	5.2	1.4	6.3	21.3	15.3	0.4	4.9	FR
P-SC	3	579.0	3.6	1,708.3	5.9	89.1	4.1	1.9	9.5	14.3	4.3	0.3	6.1	FR
P-FC	3	472.8	5.7	1,985.3	1.1	88.9	6.0	2.0	8.8	28.9	15.2	0.8	4.3	FR

Figure 5 Direct tension results for, (a) PY LY (b) PF LF (C) LF and PF with different impregnation strategies (see online version for colours)

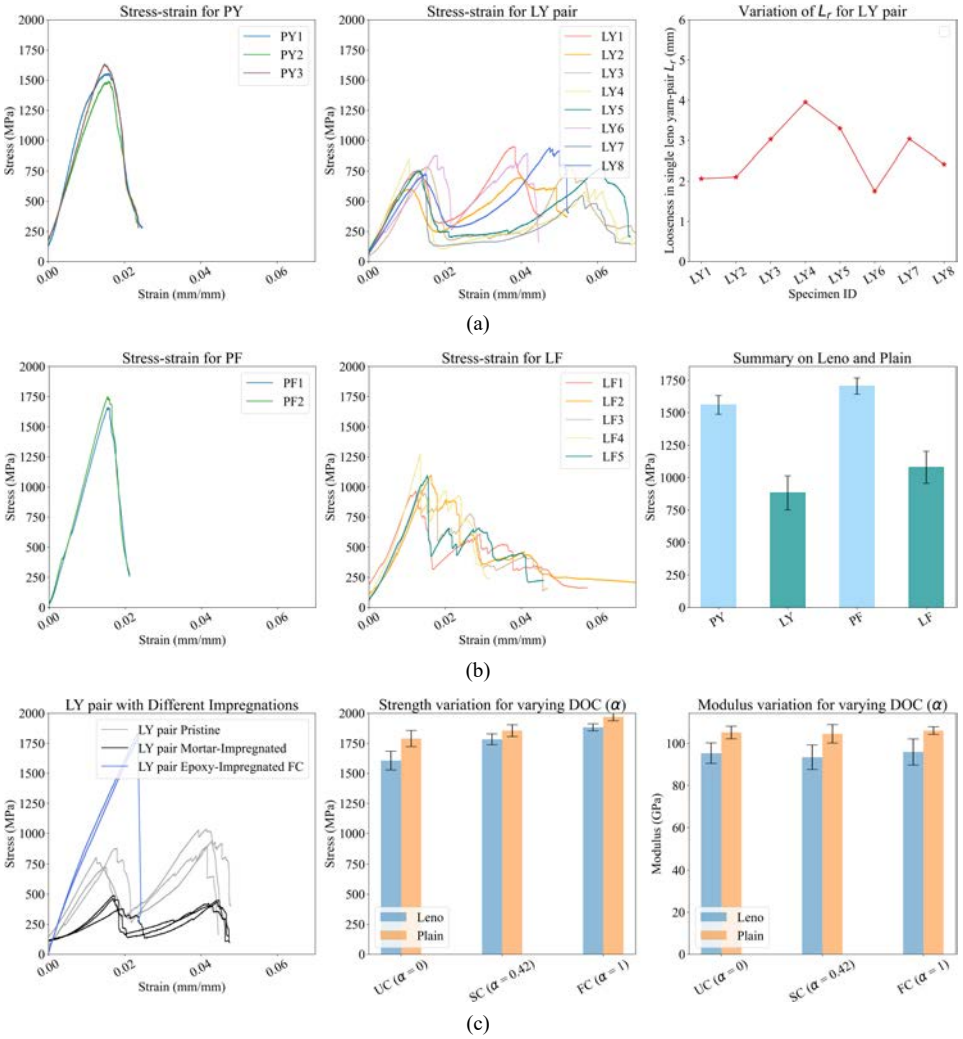

The complete test matrix data can be found in Table 6, summarising various parameters such as the first cracking stress (σ_1), ultimate stress (σ_3), composite modulus (E_3), failure strain (ϵ_u), average crack spacing (C_s), and average maximum crack width (C_w). Throughout the study, four types of failure modes were observed, including fibre-fibre slip (FFS), fibre-matrix debonding (FMD), fibre pullout (FP), and fibre rupture (FR).

4.1.2.1 Leno series

Leno specimens with pristine fibre condition (L-P) exhibit σ_3 values close to σ_1, ranging from 406.2–554.9 MPa with a coefficient of variation (COV) of approximately 10%. This indicates that the contribution of fibre mesh post-matrix cracking is insignificant. The composite modulus (E_3) is around 0.1 GPa with a COV of 26.6%. Similar

behaviour is observed in leno intersection coated (L-IC) specimens, where the fabric is coated at the warp-weft junction with fully cured epoxy. L-IC specimens show a slight improvement in σ_3 compared to L-P, with an increase of 10.6%. L-P and L-IC specimens exhibit high failure strain values of 2.6–2.9% with a FP failure mode. The average crack spacing (C_s) is observed to be in the range of 51.6–66.1 mm, with an average crack width (C_w) of 4.5–5.8 mm. In summary, L-P and L-IC specimens show large crack widths and spacing. This behaviour is attributed to three significant factors: initial looseness/stretching, lack of impregnation, and looseness difference (L_r), resulting in a two-peak behaviour. Furthermore, post-cracking, specimens tend to tilt due to non-uniform L_r in the warp yarns, which can be observed in Figures 7(a)–7(b)-(v).

Figure 6 Results for leno FRCM composites for (a) L-P (b) L-IC (c) L-UC (d) L-SC (e) L-FC (see online version for colours)

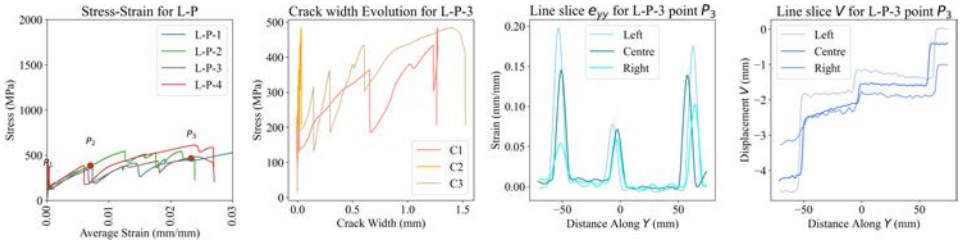

(a)

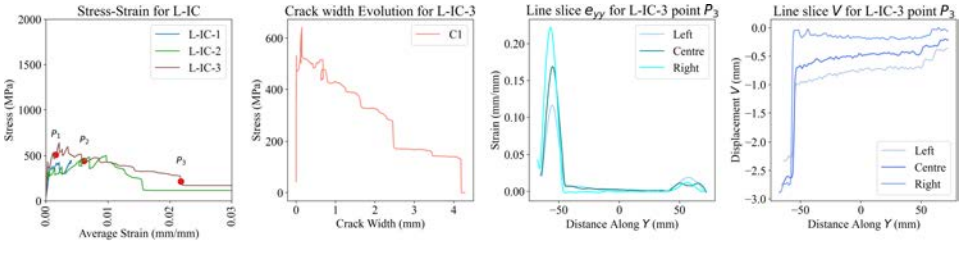

(b)

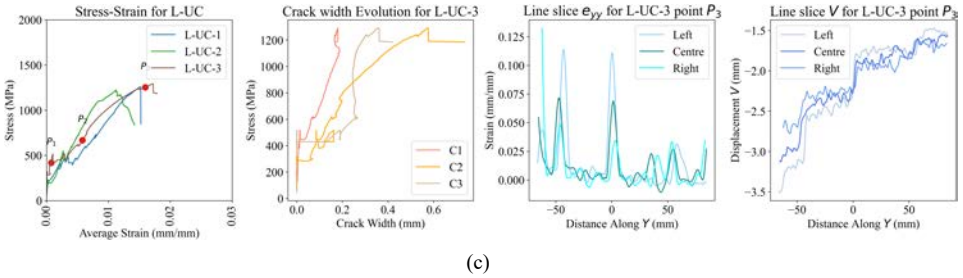

(c)

Figure 6 Results for leno FRCM composites for (a) L-P (b) L-IC (c) L-UC (d) L-SC (e) L-FC (continued) (see online version for colours)

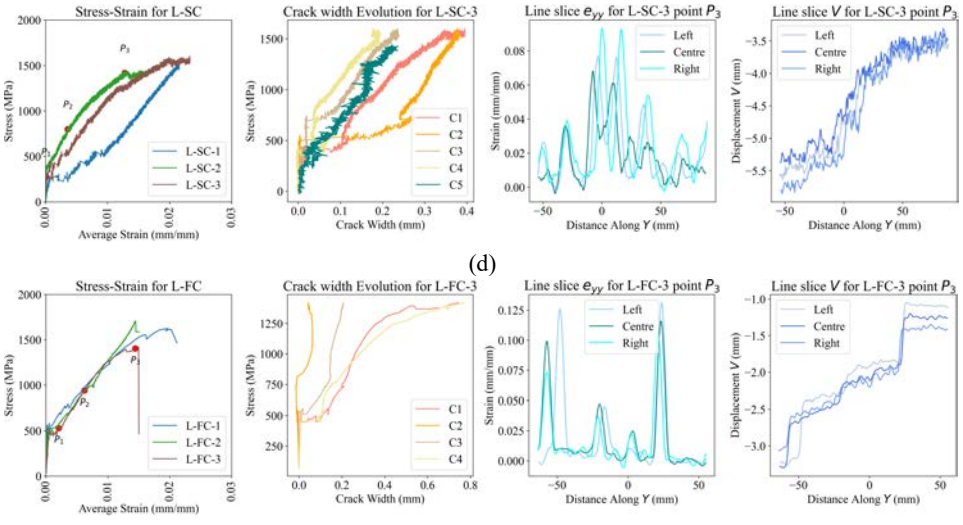

L-UC specimens are prepared by placing uncured epoxy-coated leno fabric into cement mortar. L-UC specimens show a tri-linear stress-strain response. First linear branch, followed by the multi-cracking stage, and finally cracked FRCM behaviour. The first cracking (σ_1) occurs at 392.8 MPa (COV = 2.3%), but more significantly, the specimens fail at 1,267.1 MPa with a COV of 2.7%, which is on average 116.8% higher than L-P and L-IC specimens. L-UC specimens also exhibit an average C_w of 0.7 mm and C_s of 20.1 mm. The drastic increase in ultimate capacity over L-P shows successful curing of impregnated epoxy with L-UC strategy in the mortar environment.

The epoxy-coated fabric is pre-heated in L-SC specimens until the gelation state (α = 0.42) is achieved before it is placed in mortar. The data was captured at 10 Hz accidentally, resulting in high variation as shown in Figure 6(d). L-SC specimens exhibit a nonlinear response near the ultimate stage (P_3) with a σ_3 of 1,476.8 MPa, which is 16.5% higher than L-UC. Micro-cracking is predominant throughout the stress-strain response, and failure occurs when some cracks reach a C_w of 0.5 mm with a C_s of 15.2 mm. This indicates a better fibre-matrix interaction, leading to an increased number of cracks and reduced crack spacing and width. In post-failure observation, the fabric in L-SC specimens is found to have a thin mortar layer all around. This is further explained in Subsection 4.3.2.

L-FC specimens are epoxy-coated FRCM specimens, where fully cured epoxy fabric is inserted between the mortar layers. A typical trilinear stress-strain response is observed, with σ_1 and σ_3 values of 489.9 and 1,588.4 MPa, respectively. C_w and C_s are measured to be 0.9 mm (COV 8.1%) and 26.1 mm (COV 6.7%), respectively. The overall increase in σ_3 for UC, SC, and FC specimens compared to L-P and L-IC is 116.8%, 152.7%, and 171.8%, respectively. Similarly, the damage caused by a partial DOC for UC and SC specimens relative to FC specimens is 20.2% and 7.02%, respectively. This indicates the effectiveness of the semi-cure process. All UC, SC, and FC specimens fail due to FR with a composite modulus ranging from 81.2 to 84.6 GPa.

Therefore, it is assumed, in Subsection 4.2, that the modulus of FRCM composites does not change with the initial DOC.

Figure 7 DIC visualisation for leno FRCM composites mapping to Figure 6 showing (i) P_1 point e_{yy} (ii) P_2 point e_{yy} (iii) P_3 point e_{yy} (iv) P_3 point V (see online version for colours)

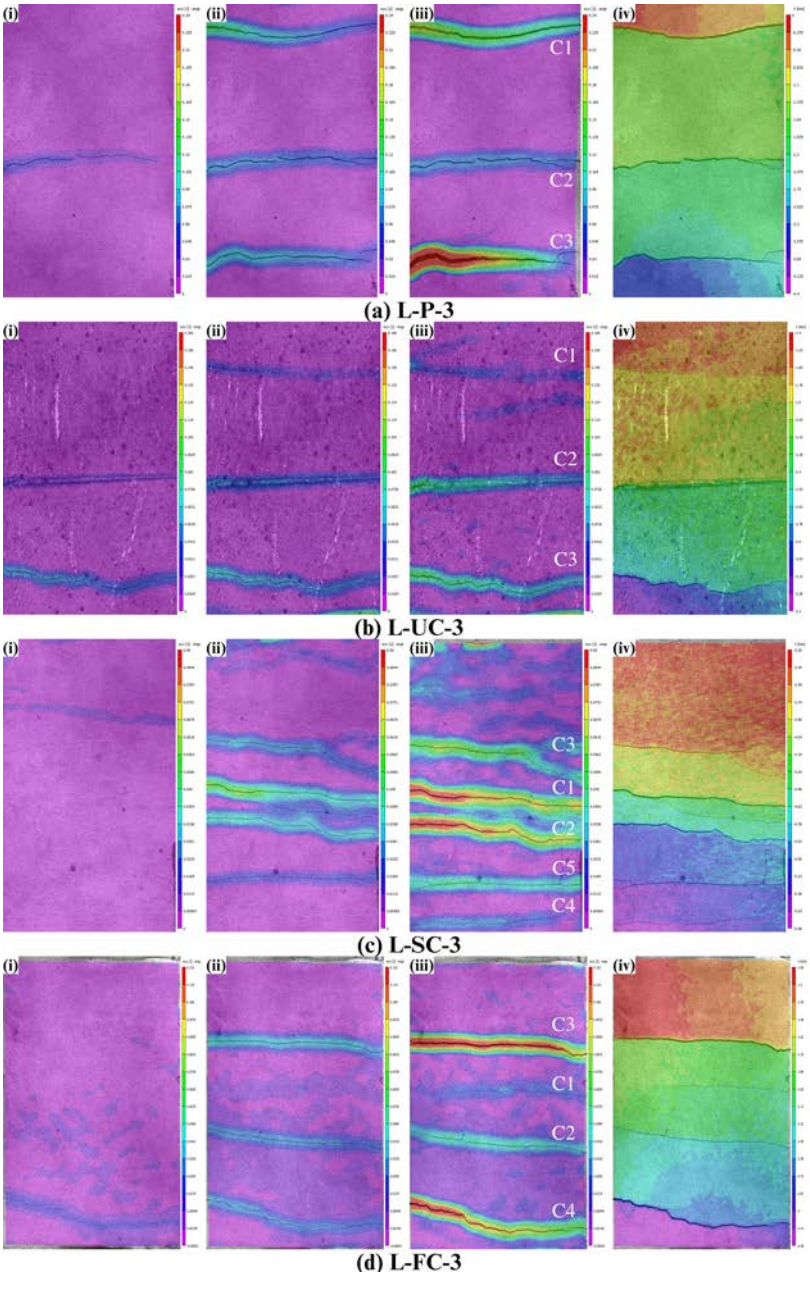

4.1.2.2 Effect of high temperature on L-SC

To further evaluate the performance of L-SC specimens, they undergo a 24-hour exposure to elevated temperatures. All high-temperature (HT) specimens exhibit a 34.4% reduction in the first cracking stress compared to room-temperature (RT) specimens. While an increase in exposure temperature from RT to 150°C does not result in a change in the σ_3 value, a decrease in ultimate capacity of approximately 16.2% is observed for the 200°C exposure, accompanied by a shift in failure mode from FR to FMD. Moreover, when L-SC specimens are exposed to 200°C, the crack width (C_w) increases from 0.5 mm to 10.8 mm, and the crack spacing (C_s) increases from 15.2 mm to 41.8 mm, indicating degradation.

Figure 8 Results for L-SC FRCM composites subjected to high-temperature for, (a) L-SC-HT100 (b) L-SC-HT150 (c) L-SC-HT200 (see online version for colours)

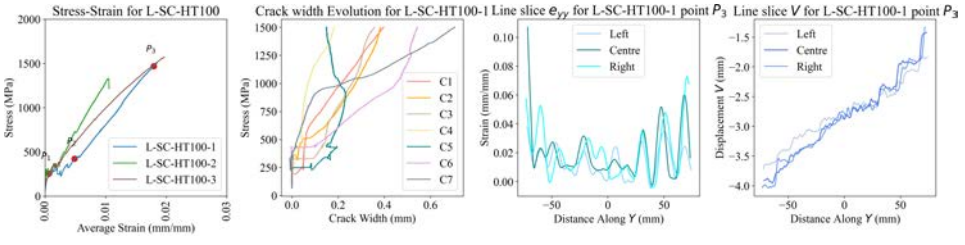

(a)

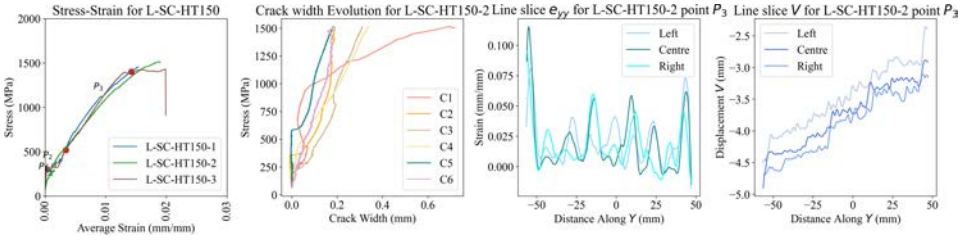

(b)

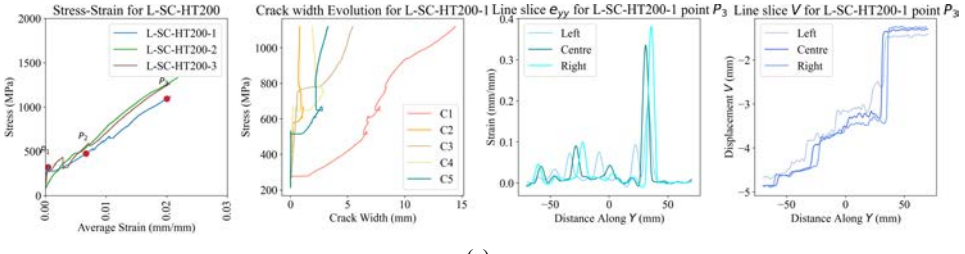

(c)

4.1.2.3 Plain series

UD plain fabric yarns exhibit consistent cross-sections along their entire length, unlike leno fabric, where the circular cross-section transforms into an elliptical shape at each warp-weft junction. Moreover, the absence of weft yarns in UD Plain fabric increases its reliance on the bond between fibres and the matrix when subjected to uniaxial

loading. Surprisingly, P-P specimens display a σ_3 value of 1,381.5 MPa (COV = 4.9%) and experience failure due to FFS. Throughout the loading process, uniform cracking is observed, with crack widths (C_w) and spacing (C_s) measuring 0.7 mm and 23.6 mm, respectively. Increasing the initial curing degree from α = 0 to α = 1 results in an increase in σ_3 from 1,605.5 to 1,985.3 MPa, accompanied by an average E_3 of 88.7 GPa. This highlights that partial curing has a positive impact on enhancing the ultimate strength of plain FRCM, ranging from 16.2–23.6% improvement compared to P-P specimens. Additionally, P-SC specimens exhibit reduced crack widths (C_w) and spacing (C_s) of 0.3 mm and 14.3 mm, respectively, indicating an improved interface bond between the fabric and matrix, similar to the behaviour observed in L-SC specimens. For all plain specimens, the first cracking (σ_1) occurs within the range of 472.8–590.8 MPa, with a COV of 3.1–5.7%.

Figure 9 Results for plain FRCM composites for, (a) P-P (b) P-UC (c) P-SC (d) P-FC (see online version for colours)

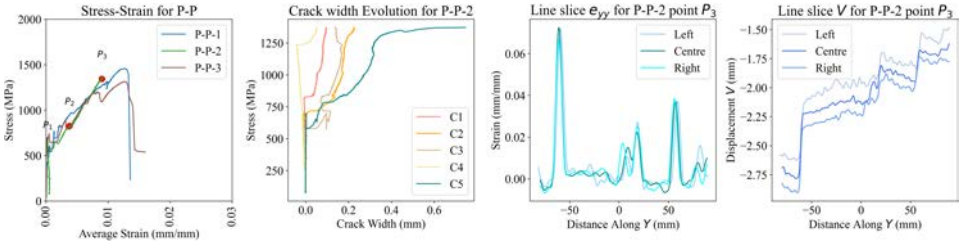

(a)

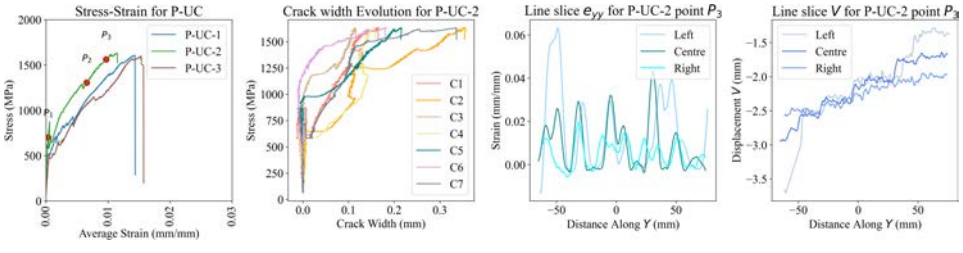

(b)

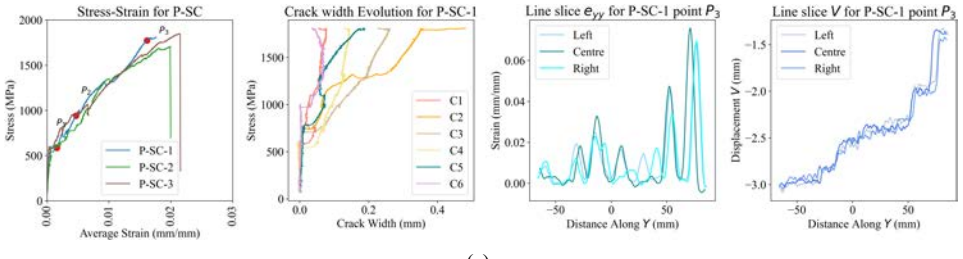

(c)

Figure 9 Results for plain FRCM composites for, (a) P-P (b) P-UC (c) P-SC (d) P-FC (continued) (see online version for colours)

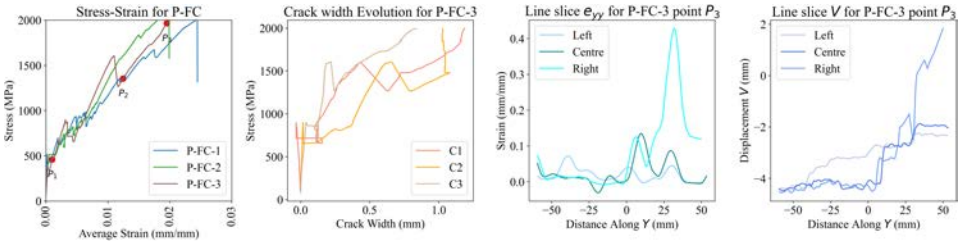

(d)

4.2 Thereotical models

4.2.1 Modified ACK

The ACK model was successfully utilised for FRCM tensile stress-strain response by Larrinaga et al. (2014) and Su et al. (2022). In this model, the tensile response is approximated as a trilinear curve. The matrix properties dominate the first stage, the second stage denotes multi-cracking, and fabric properties dominate the third stage. The rule of mixtures law using the strength of materials approach as per micromechanics (Mobasher, 2012) defines the slope of the first stage as:

$$E_I = E_m V_m + E_f V_f \tag{2}$$

E_m and E_f are the tensile moduli of elasticity of mortar and fabric, respectively, and V_m and V_f are the corresponding volume fractions. The first cracking stress, which defines the completion of stage I, is given by:

$$\sigma_{I,ACK} = \frac{E_I \cdot f_{mt}}{E_m} \tag{3}$$

where f_{mt} denotes the tensile strength of the mortar. Stage II is dominated by the formation of multiple cracks that span the length of the composite.

$$\varepsilon_{II,ACK} = (1 + 0.66 \cdot \alpha_e) \frac{f_{mt}}{E_m} \tag{4}$$

The weighted homogenisation coefficient is denoted by:

$$\alpha_e = \frac{E_m V_m}{E_f V_f} \tag{5}$$

Fabric properties dominate stage III, and its modulus is given by:

$$E_{III,ACK} = E_f V_f \tag{6}$$

Figure 10 DIC visualisation for plain FRCM composites mapping to Figure 8 showing (i) P_1 point e_{yy} (ii) P_2 point e_{yy} (iii) P_3 point e_{yy} (iv) P_3 point V (see online version for colours)

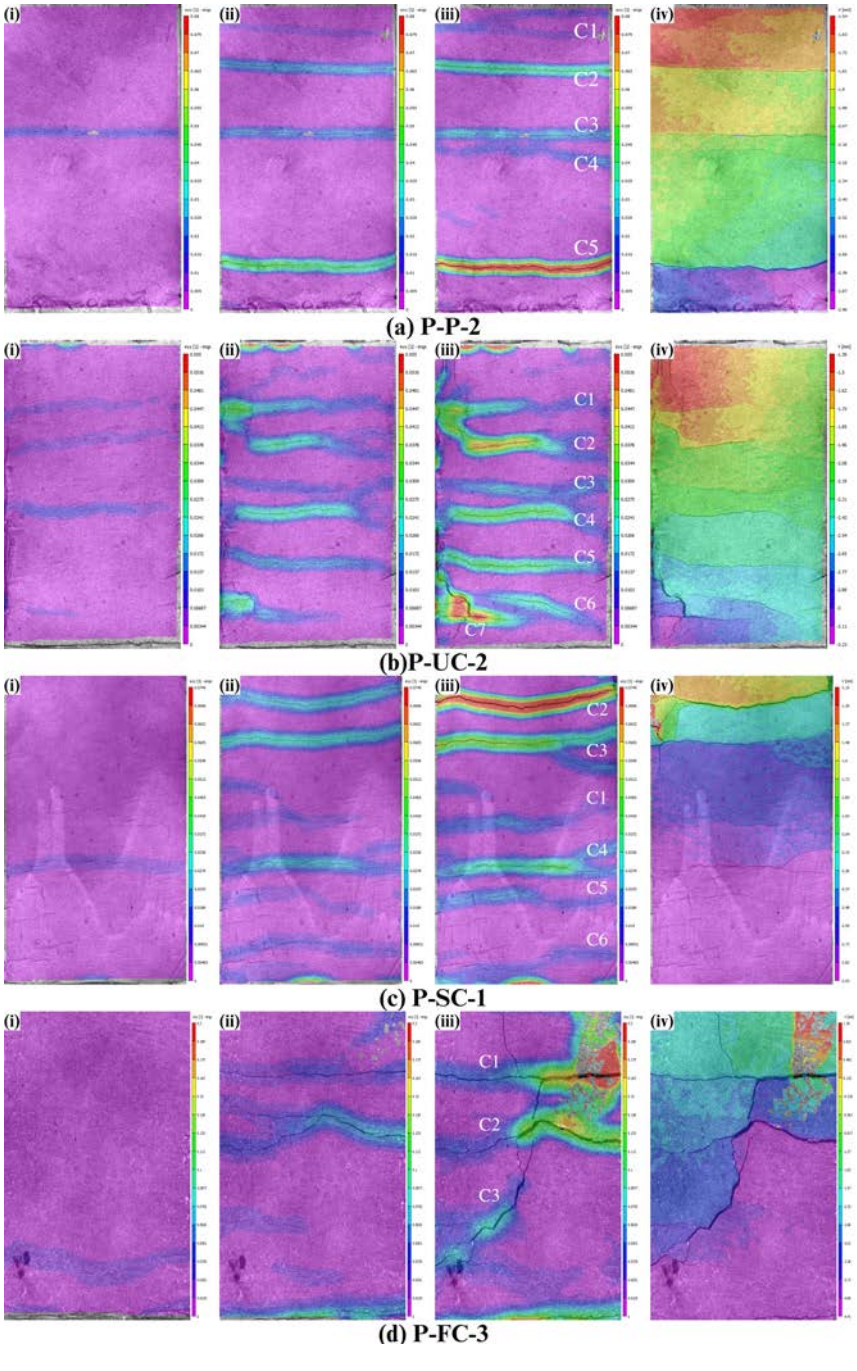

ACK model does not define the ultimate failure point, i.e., $\sigma_I II$. This limitation is overcome using the modified ACK approach proposed by Minafò and Mendola (2018). First, cracking stress is given by:

$$\sigma_{I,ModACK} = \frac{(A_m + nA_f) \cdot f_{mt}}{A_m + A_f} \tag{7}$$

where A_m and A_f denote the cross-section area of mortar and fabric, respectively, in the warp direction. The homogenisation coefficient, also known as the modular ratio, is given by $n = E_f/E_m$. Corresponding cracking strain is used instead of E_I to define the first stage as:

$$\varepsilon_{I,modACK} = \frac{f_{mt}}{E_m} \tag{8}$$

Stage II for constant load plateau is followed the same as the ACK model given by equations (4) and (5). For stage III, instead of E_{III}, ultimate strength of FRCM is defined as:

$$\sigma_{III,modACK} = f_{mt}V_m + f_tV_f \tag{9}$$

where f_t is the tensile strength of the fabric.

4.2.2 Modified tension stiffning

The tension stiffening model is a two-stage model in which the first linear stage corresponds to the cracking of the matrix, and the second hyperbolic stage defines the combined crack progression and failure of the FRCM. Nerilli and Ferracuti (2021) proposed a modified tension stiffening model and tuned the model parameters using experimental data available in the literature defined as:

$$\varepsilon(\sigma_f) = \begin{cases} \frac{\sigma_f}{\bar{E}_1} & \text{if } 0 \le \sigma_f \le \bar{\sigma}_1 \\ \frac{\sigma_f}{\bar{E}_3}\left[1 - \left(\frac{\bar{\sigma}_1}{\sigma_f}\right)^{1.51}\right] + \frac{\sigma_f}{\bar{E}_1}\left(\frac{\bar{\sigma}_1}{\sigma_f}\right)^{1.51} & \text{if } \bar{\sigma}_1 < \sigma_f \le \bar{\sigma}_3 \end{cases} \tag{10}$$

This model takes the input of equivalent model parameters derived using mechanical properties of constituent materials as $\bar{E}_1 = 0.74\left(\frac{E_m}{\rho_f} + E_f\right)$, $\bar{E}_3 = 0.88\ E_f$, $\bar{\sigma}_1 = 0.5\ \frac{f_{mt}}{\rho_f}$, and $\bar{\sigma}_3 = 0.87\ f_t$. Here ρ_f represents the fabric reinforcement ratio given by $\frac{A_f}{A_m + A_f}$.

4.2.3 Damage coefficient (d_c) and model fitting

The effect of initial DOC on FRCM stress-strain response is tuned by introducing a damage coefficient d_c [equation (11)] for ultimate strength. As noted in Subsection 4.1.2, modulus in stage III, E_3, does not change with the change in the initial DOC and affects only σ_3. Therefore, the d_c value is proposed for tuning σ_3 based on current experimental data as Figure 11(d). Damage is assessed with respect to σ_3 for the fully cured FRCM composite denoted by σ_{FC}.

$$d_c = 0.8 + 0.2\alpha \tag{11}$$

The fitted model is shown in Figure 12. Modified ACK is represented with a dotted black line, and the modified tension stiffening proposed by Nerilli and Ferracuti (2021) is indicated by a dotted red line. The modified tension stiffening model by Nerilli and Ferracuti (2021) is observed to fit the leno and plain data with an average R_2 of 94% and 95.6%, respectively.

Figure 11 (a) DSC dynamic and isothermal scans (b) DOC and tuning of damage coefficient d_c (see online version for colours)

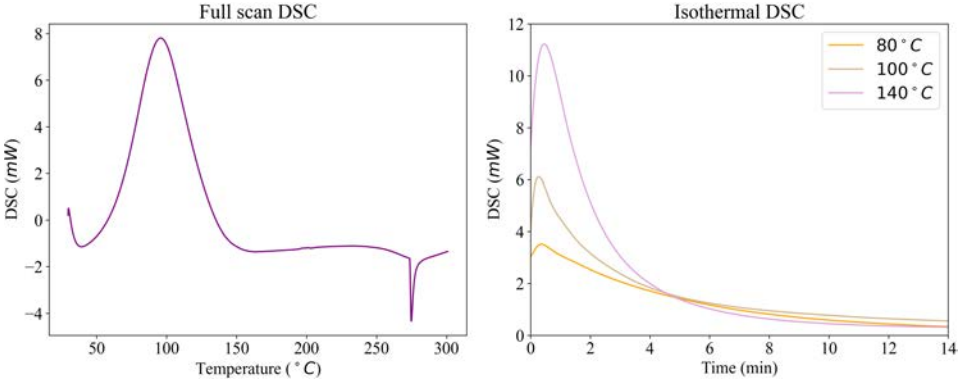

(a)

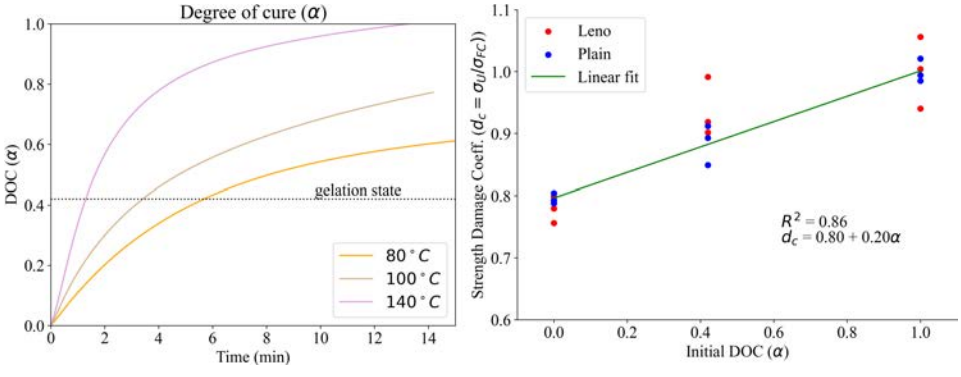

(b)

4.3 Semi-cure process

In the presence of moisture (available in mortar), the hardener reacts with the hydroxyl functional group on the resin to form a byproduct (in this case amine blush). If the amount of water increases, it can lead to excessive consumption of hardener, reducing the amount of available hardener for the reaction with the resin. This can result in incomplete curing of the epoxy matrix and a reduction in tensile strength. The semi-cure process limits the availability of unreacted hardener that can interact with water in the FRCM composite, resulting in improved overall behaviour. ESEM analysis reveals the formation of a bonded mortar layer around the specimens subjected to the semi-cure process, indicating enhanced bonding at the fibre-matrix interface. Differential scanning

calorimetry (DSC) data is utilised to optimise the semi-cure process and determine the time needed to reach the gelation state. Laser Raman spectroscopy (LRS) investigation demonstrates the effect on a molecular level for specimens treated with the semi-cure process compared to those subjected to the uncured method.

Figure 12 Thereotical stress-strain model fitting to FRCM with UC/SC/FC strategies (see online version for colours)

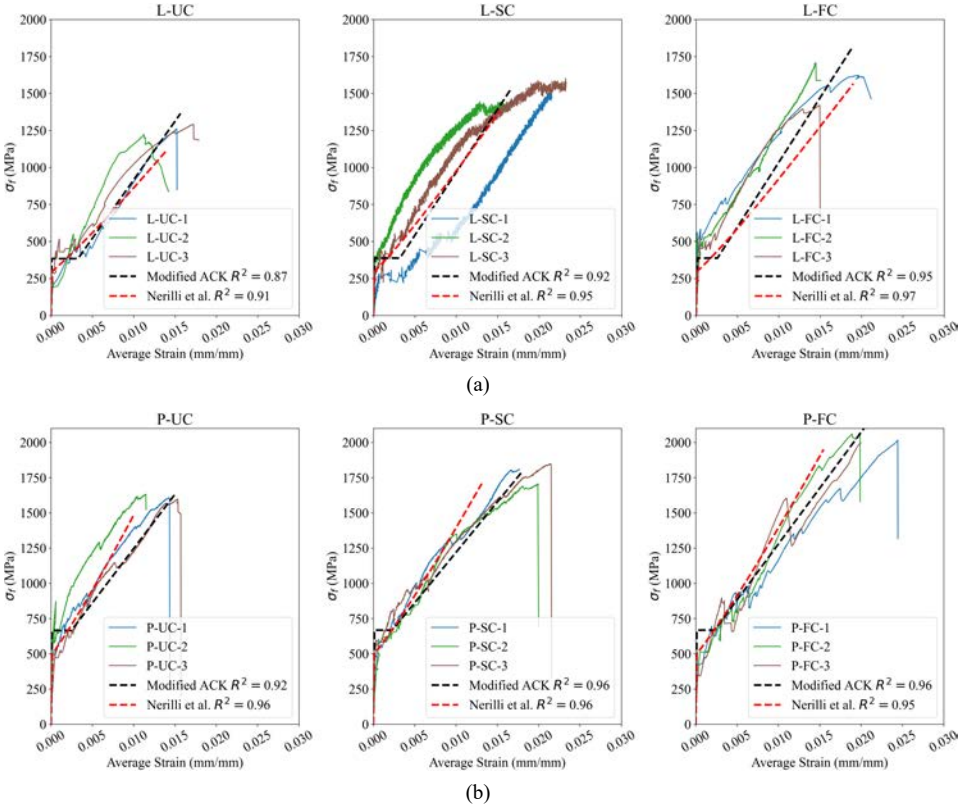

4.3.1 DSC and LRS

The results obtained from the differential scanning calorimetry (DSC) analysis are presented in Figure 11. The dynamic scan DSC reveals an exothermic behaviour of the curing reaction within the temperature range of 60°C to 140°C, with a peak observed at approximately 100°C. The gelation state of the specimens is observed at a curing degree of $\alpha = 0.42$. The LRS results, as depicted in Figure 13, illustrate the C-O-C stretch, C-C stretch, and CH_2 scissoring vibrations for the UC, SC, and FC specimens. The C-C stretch, which is particularly significant for forming epoxide rings, exhibits a peak at a wavenumber of 1,256 cm^{-1}. The intensity of this peak decreases as the DOC increases, indicating a depletion of C-C bonds. Notably, the SC specimen demonstrates a drastic reduction in the peak intensity compared to the UC specimen. Moreover, the similar shape and width of the C-C stretch peak between the SC and FC specimens indicate the absence of structural defects or other interactions that could affect the C-C vibrations.

Figure 13 LRS scans for UC/SC/FC epoxy samples as given in Figure 2(c) (see online version for colours)

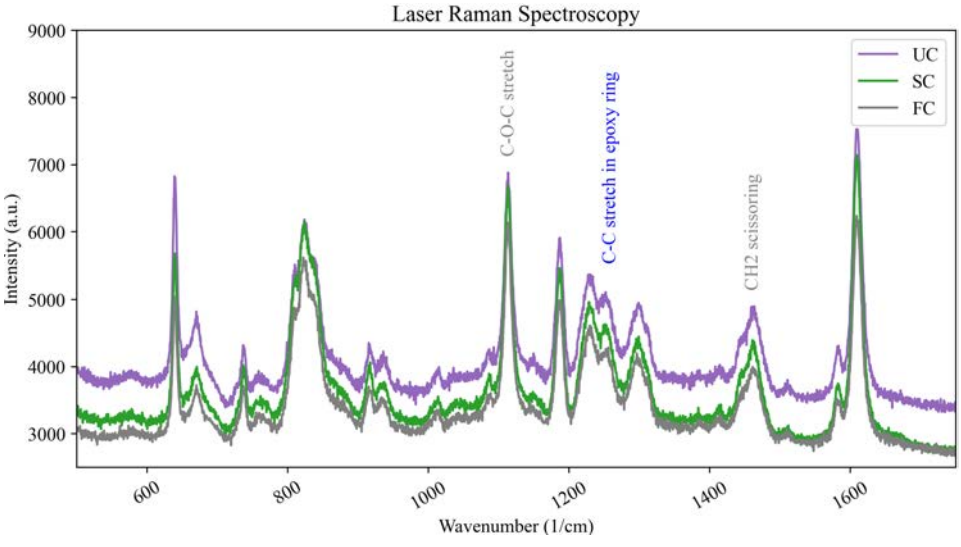

Figure 14 SEM analysis of failed samples for (a) leno (b) plain FRCM

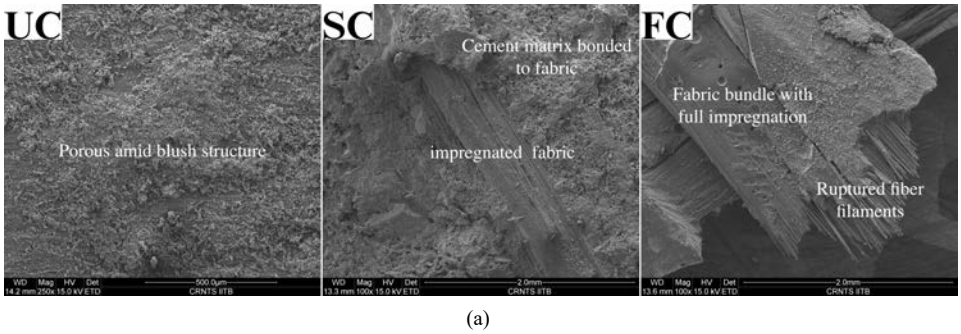

(a)

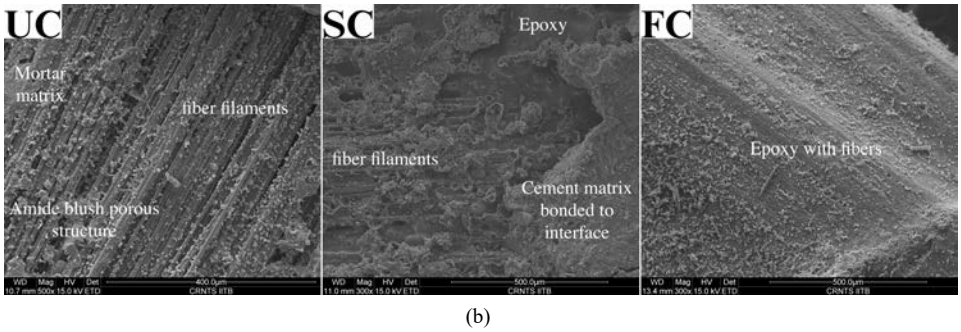

(b)

4.3.2 ESEM

ESEM analysis was conducted on the failed specimens of plain and leno FRCM composites prepared using the UC, SC, and FC strategies. The ESEM images, presented in Figure 14, provide valuable insights into the microstructural characteristics of the specimens. In the case of the UC specimens, porous structures were observed on the outer periphery of the fabric, suggesting the formation of an amide blush. This porous morphology indicates the presence of voids and poor bonding between the fabric and the mortar matrix. Conversely, the ESEM images of the SC specimens revealed the presence of mortar matrix firmly bonded to the fabric at numerous locations, indicating improved bonding behaviour at the fibre-matrix interface. This observation suggests a stronger interfacial bond and enhanced adhesion between the fabric and the mortar matrix in the semi-cured specimens.

5 Conclusions

In this investigation, we conducted a comprehensive analysis of the mechanical properties and performance of cementitious composites reinforced with both leno and plain fabrics, which had undergone varying degrees of epoxy impregnation. The key conclusions drawn from our study are as follows:

- Leno fabric specimens exhibited lower initial mechanical strength and higher elongation at the point of failure when compared to plain fabric specimens, despite possessing similar yarn properties. This discrepancy can be attributed to the inherent structural looseness of leno fabric due to its geometric configuration.
- The impregnation of leno fabric with epoxy effectively eliminated the two-peak behaviour typical of leno fabric and led to a substantial enhancement in mechanical strength. Specimens with fully cured epoxy displayed an approximately twofold increase in capacity compared to untreated leno fabric specimens.
- Our analysis of the stress-strain responses of the FRCM composites indicated variations based on the fabric type and the degree of epoxy curing. In all cases, both leno and plain fabric specimens exhibited a fibre-rupture failure mode after epoxy impregnation, regardless of the curing level.
- Partial curing of the epoxy-coated fabric demonstrated improved fibre-matrix interaction and increased ultimate strength for both leno and plain fabric composites when contrasted with untreated specimens. The semi-curing process proved effective in enhancing the mechanical properties of FRCM composites compared to untreated conditions.
- Elevated-temperature exposure of semi-cured leno fabric specimens resulted in a reduction in first cracking stress, along with increased crack width and spacing, indicating the influence of elevated temperatures on composite performance. Notably, a significant reduction in ultimate strength was observed at temperatures exceeding 200°C. Temperatures up to 150°C were deemed safe for semi-cured FRCM composites, as there was no degradation in tensile strength within this range.

- The stress-strain responses of both leno and plain FRCM composites, across various degrees of curing, were effectively described by the modified ACK and tension stiffening model proposed by Nerilli et al. This model accurately approximated the mechanical behaviour of these composites.

In summary, our study provides valuable insights into the mechanical characteristics and performance of epoxy-coated leno and plain fabric-reinforced cementitious composites. The results underscore the significance of epoxy impregnation with partial curing in enhancing the strength and overall behaviour of FRCM composites in comparison to untreated or prepreg specimens. Furthermore, the developed models offer a valuable tool for predicting the mechanical response of FRCM composites under tensile loading, aiding in their design and application in structural strengthening and repair endeavours.

Acknowledgements

The authors wish to thank the AMTF, Sophisticated Analytical Instrument Facility (SAIF), Heavy Structures Lab (HSL), and Structural Evaluation and Material Testing Lab (SEMT) at IITB for providing the equipment support for the mechanical and microstructural evaluation. Also, the authors thank Sanrachana Structural Strengthening Pvt. Ltd., Mumbai, for generously providing leno fabric (SRM C Wrap 400 BD mesh). Any views, results, conclusions, or recommendations stated in this study are those of the authors and do not necessarily contemplate the sponsoring entities.

References

Al-Salloum, Y.A., Hussein, Elsanadedy, M., Saleh, Alsayed, H. and Iqbal, R.A. (2012) 'Experimental and numerical study for the shear strengthening of reinforced concrete beams using textile-reinforced mortar', DOI: 10.1061/(ASCE)CC.1943.

American Concrete Institute (2017) *ACI 440.2R-17: Guide for the Design and Construction of Externally Bonded FRP Systems for Strengthening Concrete Structures*, American Concrete Institute, Farmington Hills, MI, USA.

ASTM International (2008) *ASTM D3039/D3039M-08: Standard Test Method for Tensile Properties of Polymer Matrix Composite Materials*, ASTM International, West Conshohocken, PA, USA.

ASTM International (2017) *ASTM D4018-17: Standard Test Methods for Properties of Continuous Filament Carbon and Graphite Fiber Tows*, ASTM International, West Conshohocken, PA, USA.

D'Ambrisi, A. and Focacci, F. (2011) 'Flexural strengthening of RC beams with cement-based composites', *Journal of Composites for Construction*, Vol. 15, pp.707–720, DOI: 10.1061/(asce)cc.1943-5614.0000218.

D'Antino, T., Calabrese, A.S. and Poggi, C. (2020) 'Experimental procedures for the mechanical characterization of composite reinforced mortar (CRM) systems for retrofitting of masonry structures', *Materials and Structures/Materiaux et Constructions*, Vol. 53, No. 8, DOI: 10.1617/s11527-020-01529-1.

Donnini, J., Corinaldesi, V. and Nanni, A. (2016) 'Mechanical properties of frcm using carbon fabrics with different coating treatments', *Composites Part B: Engineering*, Vol. 88, pp.220–228, DOI: 10.1016/j.compositesb.2015.11.012.

Dvorkin, D. and Peled, A. (2016) 'Effect of reinforcement with carbon fabrics impregnated with nanoparticles on the tensile behavior of cement-based composites', *Cement and Concrete Research*, Vol. 85, pp.28–38, DOI: 10.1016/j.cemconres.2016.03.008.

Escrig, C., Gil, L. and Bernat-Maso, E. (2017) 'Experimental comparison of reinforced concrete beams strengthened against bending with different types of cementitious-matrix composite materials', *Construction and Building Materials*, Vol. 137, pp.317–329, DOI: 10.1016/j.conbuildmat.2017.01.106.

European Committee for Standardization (2016) *EN 196-1:2016 (E): Methods of Testing Cement – Part 1: Determination of Strength*, European Committee for Standardization, Avenue Marnix 17, B-1000 Brussels, Belgium.

Ferreira, K.F., Rampini, M.C., Zani, G., Colombo, M. and di Prisco, M. (2023) 'Experimental investigation on the use of fabric-reinforced cementitious mortars for the retrofitting of reinforced concrete dapped-end beams', *Structural Concrete*, DOI: 10.1002/suco.202200743.

Guo, L., Deng, M., Li, R., Li, T. and Dong, Z. (2022) 'Shear strengthening of RC short columns with CFRP grid-reinforced FRC matrix: cyclic loading tests', *Journal of Building Engineering*, October, Vol. 47, p.103915, DOI: 10.1016/j.jobe.2021.103915.

Halvaei, M., Latifi, M. and Jamshidi, M. (2018) 'Study of the microstructure and flexural behavior of cementitious composites reinforced by surface modified carbon textiles', *Construction and Building Materials*, Vol. 158, pp.243–256, DOI: 10.1016/j.conbuildmat.2017.10.044.

Heins, K., Lesker, S., Pütz, J., Hüntemann, M. and Gries, T. (2023) 'Effect of thermoplastic impregnation on the mechanical behaviour of textile reinforcement for concrete', *SN Applied Sciences*, Vol. 5, No. 3, DOI: 10.1007/s42452-023-05305-y.

Hojdys, U. and Krajewski, P. (2021) 'Tensile behaviour of FRCM composites for strengthening of masonry structures – an experimental investigation', *Materials*, Vol. 14, No. 13, DOI: 10.3390/ma14133626.

ICC Evaluation Services Inc. (2016) *AC434: Masonry and Concrete Strengthening Using Fabric-reinforced Cementitious Matrix (FRCM) and Steel Reinforced Grout (SRG) Composite Systems*, ICC Evaluation Services Inc., Los Angeles, CA, USA.

Larrinaga, P., Chastre, C., Biscaia, H.C. and San-José, J.T. (2014) 'Experimental and numerical modeling of basalt textile reinforced mortar behavior under uniaxial tensile stress', *Materials and Design*, Vol. 55, pp.66–74, DOI: 10.1016/j.matdes.2013.09.050.

Messori, M., Nobili, A., Signorini, C. and Sola, A. (2019) 'Effect of high temperature exposure on epoxy-coated glass textile reinforced mortar (GTRM) composites', *Construction and Building Materials*, Vol. 212, pp.765–774, DOI: 10.1016/j.conbuildmat.2019.04.026.

Minafò, G. and Mendola, L.L. (2018) 'Experimental investigation on the effect of mortar grade on the compressive behaviour of FRCM confined masonry columns', *Composites Part B: Engineering*, Vol. 146, pp.1–12, DOI: 10.1016/j.compositesb.2018.03.033.

Mobasher, B. (2012) *Mechanics of Fiber and Textile Reinforced Cement Composites*, CRC Press, Taylor & Francis Group, Boca Raton, USA.

Nadiv, R., Peled, A., Mechtcherine, V., Hempel, S. and Schroefl, C. (2017) 'Micro- and nanoparticle mineral coating for enhanced properties of carbon multifilament yarn cement-based composites', *Composites Part B: Engineering*, Vol. 111, pp.179–189, DOI: 10.1016/j.compositesb.2016.12.005.

Nerilli, F. and Ferracuti, B. (2021) 'A tension stiffening model for frcm reinforcements calibrated by means of an extended database', DOI: 10.17632/4zg9.

Ombres, L. (2011) 'Flexural analysis of reinforced concrete beams strengthened with a cement-based high strength composite material', *Composite Structures*, Vol. 94, pp.143–155, DOI: 10.1016/j.compstruct.2011.07.008.

Ombres, L. (2014) 'Concrete confinement with a cement based high strength composite material', *Composite Structures*, Vol. 109, pp.294–304, DOI: 10.1016/j.compstruct.2013.10.037.

Peled, A. and Bentur, A. (2000) 'Geometrical characteristics and efficiency of textile fabrics for reinforcing cement composites', *Cement and Concrete Research*, Vol. 30, No. 5, pp.781–790, https://doi.org/10.1016/S0008-8846(00)00239-8.

Rampini, M.C., Zani, G., Schouler, L., Colombo, M. and di Prisco, M. (2021) 'Effect of textile characteristics on the ar-glass fabric efficiency', *Textiles*, Vol. 1, pp.387–404, DOI: 10.3390/textiles1020020.

Scheurer, M., Kalthoff, M., Matschei, T., Raupach, M. and Gries, T. (2022) 'Analysis of curing and mechanical performance of pre-impregnated carbon fibers cured within concrete', *Textiles*, Vol. 2, pp.657–672, DOI: 10.3390/textiles2040038.

Signorini, C., Nobili, A., González, E.I.C. and Siligardi, C. (2018) 'Silica coating for interphase bond enhancement of carbon and AR-glass textile reinforced mortar (TRM)', *Composites Part B: Engineering*, Vol. 141, pp.191–202, DOI: 10.1016/j.compositesb.2017.12.045.

Signorini, C., Nobili, A., Sola, A. and Messori, M. (2020) 'Optimal epoxy dilution for epoxy-coated textile reinforced mortar (TRM): an experimental perspective', in Carcaterra, A., Paolone, A. and Graziani, G. (Eds.): *Proceedings of XXIV AIMETA Conference 2019*, Springer International Publishing, Cham, pp.499–511.

Su, M.N., Wang, Z. and Ueda, T. (2022) 'Optimization and design of carbon fabric-reinforced cementitious matrix composites', *Structural Concrete*, Vol. 23, pp.1845–1860, DOI: 10.1002/suco.202000801.

Tello, N., Abed, F., ElRefai, A., El-Maaddawy, T and Alhoubi, Y. (2023) 'Experimental investigation of pre-damaged circular RC columns strengthened with fabric-reinforced cementitious matrix (FRCM)', *Structural Concrete*, Vol. 24, pp.1656–1669, DOI: 10.1002/suco.202200333.

Tetta, Z.C., Koutas, L.N. and Bournas, D.A. (2016) 'Shear strengthening of full-scale RC T-beams using textile-reinforced mortar and textile-based anchors', *Composites Part B: Engineering*, Vol. 95, pp.225–239, DOI: 10.1016/j.compositesb.2016.03.076.

Trapko, T. (2013) 'The effect of high temperature on the performance of CFRP and FRCM confined concrete elements', *Composites Part B: Engineering*, Vol. 54, pp.138–145, DOI: 10.1016/j.compositesb.2013.05.016.

Tsesarsky, M., Peled, A., Katz, A. and Anteby, I. (2013) 'Strengthening concrete elements by confinement within textile reinforced concrete (TRC) shells – static and impact properties', *Construction and Building Materials*, Vol. 44, pp.514–523, DOI: 10.1016/j.conbuildmat.2013.03.031.

Younis, A., Ebead, U. and Shrestha, K. (2020) 'Tensile characterization of multi-ply fabric-reinforced cementitious matrix strengthening systems', *Structural Concrete*, Vol. 21, pp.713–723, DOI: 10.1002/suco.201900076.

Zhu, D., Bai, X., Yao, Q., Rahman, M.Z., Li, X., Yang, T. and Guo, S. (2023) 'Effects of volume fraction and surface coating of textile yarns on the tensile performance of AR-glass textile reinforced concrete', *Journal of Building Engineering*, Vol. 71, p.7, DOI: 10.1016/j.jobe.2023.106420.